Aerodynamic Effects of Phase Offset Between Synchronized Propellers in Hover

Nathan Welker * and Daniel Maynes †
Brigham Young University, Provo, Utah 84602

Emerging advances in electric-propulsion technology are enabling aircraft to use distributed electric propulsion (DEP) to increase performance and maneuverability. Distributed electric propulsion can also provide unique take-off and landing abilities which are not commonly found on traditional aircraft. The implementation of DEP effectively decreases the spacing between propellers, introducing complex aerodynamic interactions that are not well understood. This study aims to present the findings of the effects of phase offset on the flow fields of synchronized propellers at close-proximity using a particle image velocimetry system. The tip vortex locations and peak vorticities were tracked and plotted for various phase offset cases. The tip vortices of the dual propeller cases were found to decay more rapidly than the single propeller case. The momentum flux was integrated across the stereoscopic velocity field and compared between the phase offset tests. When compared to the single propeller test, fluctuations of up to 5% were found for the dual propeller cases. Traditional thrust measurements were used to validate this method. When compared to the thrust measurements, the momentum flux was consistently 6-8% lower than the thrust measurements, which is hypothesized to be due to not accounting for pressure acting on the control surface. The results of this work suggests that the potential benefits of controlling propeller phase offset can be realized with negligible effects on propeller flow features and thrust fluctuations.

I. Introduction

Developments in aviation technology are creating new opportunities to use distributed electric propulsion (DEP) on novel aircraft concepts in support of urban air mobility (UAM). The propulsion system for DEP vehicles spread many small electric motors and propellers around the aircraft. Unlike jet engines or turbines, scaling electric motors up or down in size results in almost no difference in power-to-weight ratio or efficiency, making DEP advantageous over conventional aircraft designs [1]. The use of DEP has many potential advantages, including increased efficiency. For example, NASA's Greased Lightning (GL-10) concept demonstrated a 75% increase in aerodynamic performance when compared to a traditional helicopter [2]. Other advantages include increased maneuverability, better structural loading

*Doctoral Candidate, Department of Mechanical Engineering; nwelker@byu.edu
†Professor, Department of Mechanical Engineering; maynes@byu.edu

distribution, increased lift, and electric vertical take-off and landing (eVTOL) capabilities [1, 3–5].

Despite the benefits over traditional propulsion systems, the inevitable decrease of propeller spacings on DEP vehicles causes complex interactions that can be detrimental, with some researchers reporting thrust fluctuations, decreased performance, and large noise signatures [6–14]. One such study was performed by Zhou et al. [15] and Ning [16] who used a stereoscopic particle image velocimetry (SPIV) system and dynamic load measurements to determine the effects of rotor-to-rotor interactions on the aerodynamic performance of small unmanned aerial vehicles (UAVs). They concluded that thrust fluctuations would increase dramatically as the separation distance decreased, with fluctuations as high as ~250% for the smallest separation ($L = 0.05D$), twin-rotor case when compared to the single-rotor case. A decrease in rotor spacing from $L = 1.0D$ to $L = 0.05D$ also resulted in a 3dB higher noise distribution. The streamtube of a single propeller control test was circular, as was expected. However, in the dual rotor case, the flow was neither circular nor symmetric and a region of flow separation and induced upwash was shown in the results of their work. The separation and upwash are likely due to the rotor-to-rotor interactions and are hypothesized to be the cause for the strong thrust fluctuations and high noise distributions experienced in the dual rotor cases at small separation distances.

Others, like Shukla et al. [17] also reported detrimental interactions between the wakes and tip vortices of interacting propellers, leading to reduced performance. They noted the interactions between the propellers cause unique behavior of the major wake features. Figure 1 contains an illustration of these wake features and how small separation distances alters the flow structures. Specifically, the tip vortex strengths, structures, and trajectories are all changed as they interact with the adjacent rotor. Shukla et al. hypothesize that these blade-vortex interactions are the cause behind the decrease in performance. They suggest a setup with a mechanical linkage system to synchronize the rotation rates of the rotors to verify this hypothesis.

Particle image velocimetry (PIV) systems, such as the ones used by Zhou et al. [15], Ning [16], and Shukla et al. [17], can be powerful tools to characterize the flow fields generated by propellers. These systems use high-speed cameras to record multiple images of a particle-induced flow field illuminated by a laser at high acquisition rates [18]. Standard PIV systems utilize a single camera and can generate 2D planar velocity fields. Stereoscopic PIV systems use two cameras and are able to capture the perpendicular component of velocity in a plane. For propeller-driven flows, images of the flow field are often obtained in two ways:

1) The system is triggered externally to lock the images to specific propeller phase angles (also known as phase-locking). This data can be ensemble-averaged to capture the flow behavior at specific phase angles.
2) The images are captured at random propeller phase angles (also known as free-running). This data can be time-averaged to capture the flow behavior averaged across all phase angles.

Both forms of acquisition are often used and can provide valuable data for analysis and discussion. When exploring multirotor flows, however, many researchers have opted to phase-lock only the primary propeller, leaving the secondary

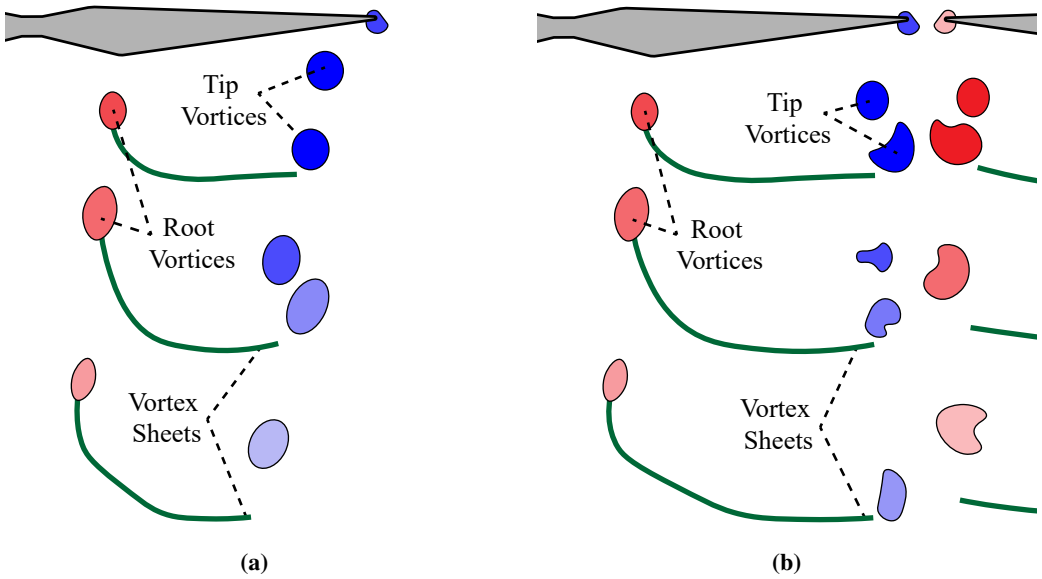

Fig. 1 A model of an instantaneous flow field with its respective features for: (a) a single propeller configuration and for (b) a dual propeller configuration.

propeller free-running [15–17]. In other words, the interacting propellers are rotating asynchronously. Although difficult to implement in practice, propeller synchronization can be invaluable in providing a greater understanding of the propeller interactions, as was suggested by Shukla et al. [17].

Synchronizing propellers in a side-by-side configuration provides the unique ability to control the relative phase offset between the propellers. Phase control between interacting propellers has proven effective at altering directivity patterns, revealing the potential to steer or reduce noise pollution in urban areas [13, 19–22]. While preliminary research suggests phase offset has a minimal impact on the time-averaged behavior of interacting propellers [13], a full aerodynamic exploration on the flow features of propellers with varying phase offsets has not been performed. Implementing a synchronized system and performing such an exploration can answer what effect, if any, phase offset has on the detrimental interference.

Thrust fluctuations are also expected to be altered with changing phase offset between interacting propellers. Measuring the thrust of side-by-side propellers spinning at high rates requires expensive measurement systems and sensors. However, according to momentum theory, measuring the fluctuations of momentum flux in the propeller wake can be synonymous with measuring thrust fluctuations. Momentum flux can be found by integrating the SPIV velocity fields across the control surface of any phase-locked experiment. This method is significant since it can be used to find fluctuations for any propeller in any side-by-side case without the use of load cells or thrust sensors. The use of momentum flux to measure thrust fluctuations, however, should be compared to actual thrust measurements to validate this method.

This study aims to explore the aerodynamic interactions between two counter-rotating, synchronized propellers in

close proximity. Using a SPIV system, the tip vortices and wake profiles of interacting propellers with varying phase offset were found, analyzed, and compared between the various phase offset cases. The integral of momentum flux was performed across the propeller wakes and compared to thrust measurements. The results of this work will provide valuable insight into the aerodynamic performance of propellers at different phase offsets.

II. Methods

A. Facility

The experimental investigations are performed in the BYU Engineering Research Lab using the large Aerolab wind tunnel at static conditions. The tunnel has a 120 mph maximum speed, a 4 ft $\times$ 3 ft $\times$ 14 ft test section, and a contraction ratio of 5:1.

B. Experimental apparatus

The experimental apparatus consists of two propeller stands housed by 3D printed aerodynamic shrouds. The shrouds are designed to provide minimal obstruction downstream of the propellers. The two shrouds are identical in shape and size but have differing internal components. One of the stands consists of a single motor which provides rotation to two DJI 9443 propellers. This shroud also contains an optical rotation sensor used to generate a cyclic signal. An external triggering device converts the cyclic signal to a Transistor-Transistor Logic (TTL) signal which is used to trigger the PIV system at specific propeller phase angles. The propeller synchronization is implemented by mechanically-linking the two propellers together with a shaft and miter gear system.

C. Measurement techniques

The high-resolution PIV system used to obtain flow-field measurements of the two propellers is outlined in Fig. 2a. A LaVision droplet generator introduces oil particles approximately 1 µm in diameter to the air flow. A double-pulsed Nd:YAG laser emitting two 200 mJ pulses with a 532 nm wavelength illuminates the particles. A high-resolution LaVision Imager Intense camera is used to obtain the PIV image pairs of the illuminated particles. For the PIV experiments, the laser is positioned to intersect the axes of the rotors. The camera is positioned to view the tip vortices and wake profiles of the propellers. The time delays between the two images are between 50 to 200 µs to provide a maximum particle displacement of of 10 pixels.

The SPIV system is outlined in Fig. 2b. This system uses the same particle generator and laser as the PIV setup, however it includes an additional camera and tilt-shift adaptors to account for the Schiemfplug principle. The cameras are positioned at an angle from the measurement plane while the laser is positioned to illuminate a plane directly downstream ($z = 0.1D$) from the propellers to provide a cross-sectional view of the propeller wakes. The same time delays between 50 to 200 µs were implemented to provide a maximum particle displacement of of 10 pixels.

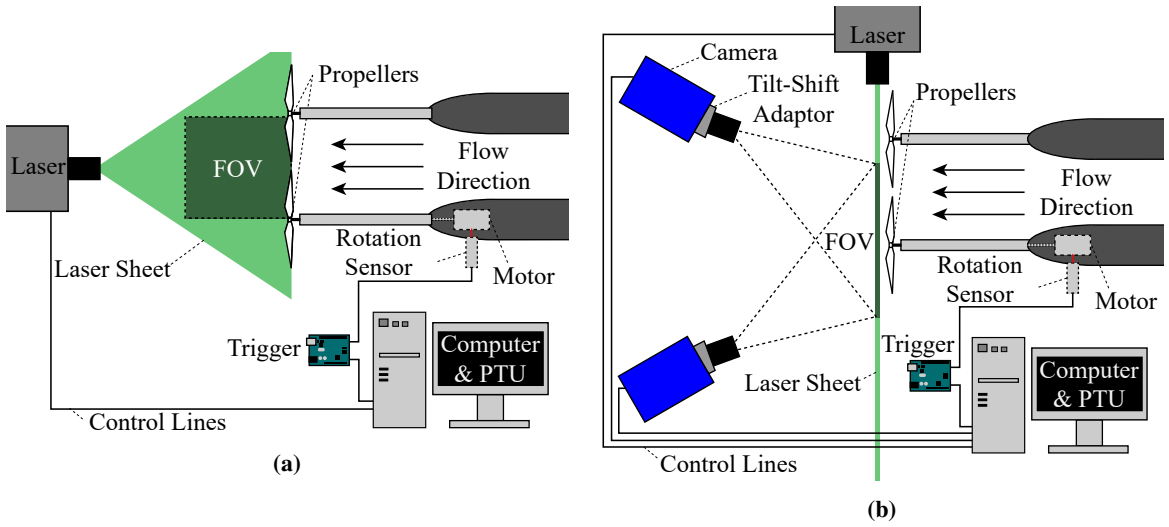

Fig. 2 The PIV (a) and SPIV (b) setups used in the experiments

1. PIV processing and uncertainty

The PIV and SPIV images are pre-processed using a subtraction filter to eliminate the background and propeller reflections. Instantaneous flow velocity vector fields are then obtained by post-processing the images. This is done by performing two passes of a cross-correlation technique with an interrogation window size of 36×36 pixels and an effective overlap of 50% followed by two passes with an interrogation window of size 16×16 and an effective overlap of 50%. The flow velocity vector fields are then ensemble averaged to obtain velocity and vorticity fields. These vector and scalar fields can be used to determine the effect of phase offset and interacting propellers on the flow features of the different propeller cases. The results of the PIV experiments were used to determine the locations and strengths of tip vortices while the results of the SPIV experiments were used to calculate the integral of momentum flux.

The uncertainties for the measured velocity fields are outlined in Table 1 and were found using the method outlined by Wieneke et al. [23].

Table 1 Overview of the max and mean uncertainty values across the measurement plane for the PIV and SPIV experiments

Case	Max Uncertainty (% of U_{tip})	Mean Uncertainty (% of U_{tip})
PIV	1.87	0.162
SPIV	2.01	0.148

2. Load measurements

The thrust measurements of the isolated propeller were performed with an RC Benchmark Series 1520 thrust stand. The thrust was acquired at 6.65 Hz while the rotation rate was acquired at 40 Hz. Tests were averaged across 30 seconds

of data acquisition. Various rotation rates were explored to compare to other published thrust data of the DJI 9443 propeller. The uncertainty of the thrust measurements were found using the 95% confidence interval of the raw thrust data, the 95% confidence interval for the RPM data, and the thrust stand tolerances. The thrust measurements were non-dimensionalized using the following thrust coefficient equation:

$$C_T = \frac{T}{\rho \pi R^2 (\omega R)^2} \tag{1}$$

where T is the propeller thrust, ρ is the air density, R is the propeller radius, and ω is the rotation rate. The results of the thrust measurements will be compared to work done by Zawodny et al. [24] and the integral of momentum flux as a form of validation for the method.

3. Integral of momentum flux

Applying a control volume analysis to a plane in the wake of a propeller yields the following form of the general linear momentum equation:

$$\sum \vec{F} = \frac{\partial}{\partial t} \int_{CV} \rho \vec{V} dV + \int_{CS} \rho \vec{V} (\vec{V}_r \cdot \vec{n}) dA \tag{2}$$

Thrust is assumed to be the only force acting on the control surface and the flow is assumed to be steady and incompressible. Using the bulk movement assumption used in PIV analysis, the velocity of each group of particles can also be assumed to be approximately uniform, meaning the integral of momentum flux can then be rewritten as a summation. Applying these assumptions yields the following equation:

$$T = \rho A_w \sum_{n=1}^{N} (\overline{w}_n^2 + w_n'^2) \tag{3}$$

where T is the propeller thrust, A_w is the area of each interrogation window (the area represented by one PIV velocity vector), ρ is the air density, and $\overline{w}$ and w' are the time-averaged and fluctuating velocity components, respectively, in the z-direction.

Using equation 3, the integral of momentum flux can be applied to the phase-locked SPIV velocity fields to obtain the thrust fluctuations as a function of phase angle. This method can also be applied to phase-averaged measurements and compared to load measurements of the previous section for validation.

D. Description of experiments

The propellers were phase locked at 30 degree increments and rotating at 4860 RPM (81 Hz). Phase angles were measured from the leading edge of the propeller starting at horizontal. For the dual propeller cases, the propellers are counter-rotating and set to a limiting separation distance ($s = 0.05D$). All cases are performed in hover condition

($J = 0$). Two limiting phase offset cases are explored (see Fig. 3):

1) The propellers have zero offset, referred to as the "dual propeller, in phase" case.

2) The propellers are at a 90° offset, referred to as the "dual propeller, out of phase" case.

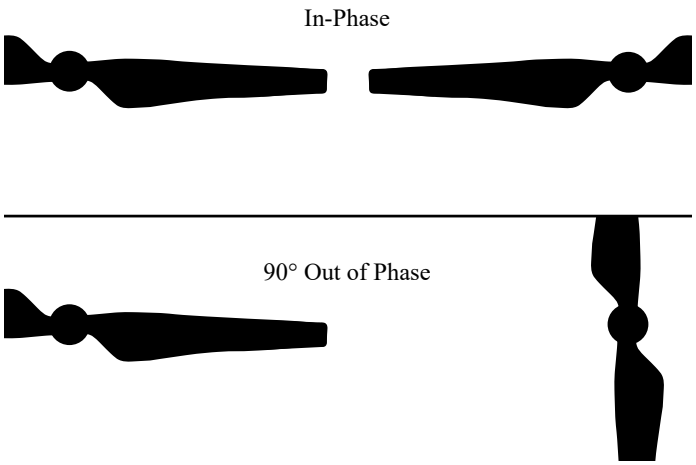

Fig. 3 Phase offset notation for the dual propeller cases.

The results of the phase offset cases will be compared to single propeller case to explore the aerodynamic effects of phase offset based on the wake flow features and tip vortex behavior.

III. Results and Discussion

A. Tip vortices

Results from the PIV tests are displayed in Fig. 4, where non-dimensional vorticity is presented. The single, dual in phase, and dual out of phase propeller cases are shown on the left, middle, and right of the figure, respectively. The propellers were phase-locked at zero degrees (horizontal). Color represents non-dimensional vorticity. The tip vortices of the dual propeller cases have a significantly faster decay in size and vorticity magnitude when compared to the single propeller tip vortices. The trajectories of the dual propeller tip vortices are also altered when compared to the single case. There is little to no difference seen between the different phase offset cases.

Plotting the locations and peak vorticity of each tip vortex for the three cases can help determine the differences in decay rates and trajectories between the three cases. The vortex locations and peak vorticity values are shown in Fig. 5a and 5b, respectively. The tip vortices of the single propeller case turn inward toward the center of the wake vortex core, settling around $x = 0.35D$. The trajectories of the tip vortices of the dual propeller cases are turned more outward, being pulled towards the secondary propeller and settling around $x = 0.45D$.

The peak vorticity of the tip vortices for all cases decays linearly. The dual propeller cases decay more quickly than the single propeller case. For both dual cases, the slope is 55% steeper than the slope of the single tip vortices,

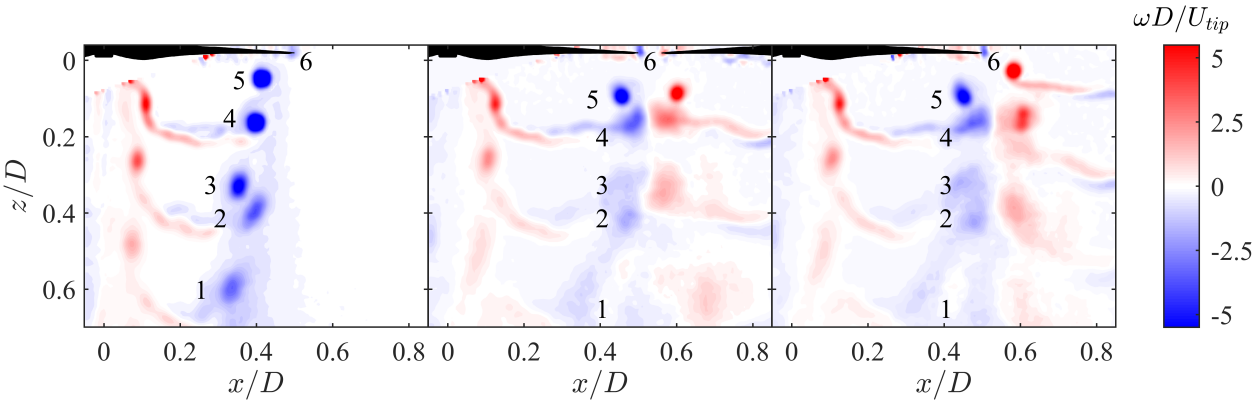

Fig. 4 Vorticity plots at a zero degree phase angle (horizontal).

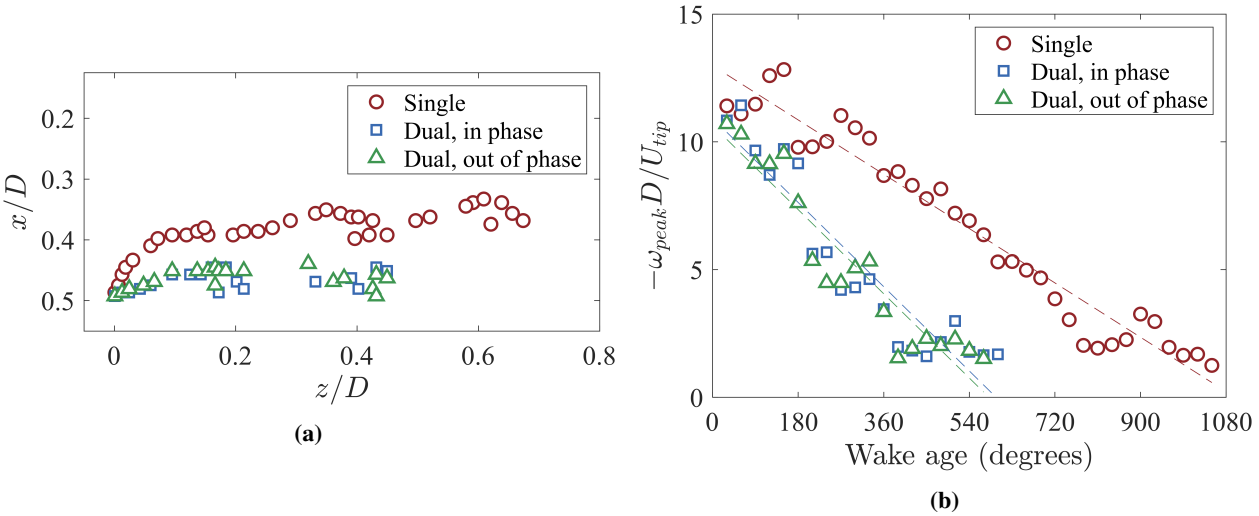

(a) **(b)**

Fig. 5 Results of the analyzed tip vortices: (a) tip vortex locations of the three propeller cases, (b) non-dimensional maximum tip vortex vorticity versus downstream distance (wake age).

approaching zero vorticity at a wake age of 600° as opposed to 1080° for the single propeller case. For both trajectories and vorticity decay, there is little to no difference between the differing phase offset cases.

B. Thrust and momentum flux

Fig. 6 shows the SPIV experiments. Similarly to Fig. 4, the single, dual in phase, and dual out of phase propeller cases are shown on the left, middle, and right of the figure, respectively, and the propellers are at a zero degree phase angle. Color represents non-dimensional axial velocity. There are little differences between the two phase angles for the single propeller case and between the phase offset tests. The largest differences arise when comparing the single propeller case to the dual propeller cases. A larger region of axial flow between the tips of the dual propellers is evident. This is similar to the findings of Zhou et al. [15], who noted that the streamtubes of interacting propellers are attracted and bent toward each other, which they hypothesized to be due to the Coanda effect.

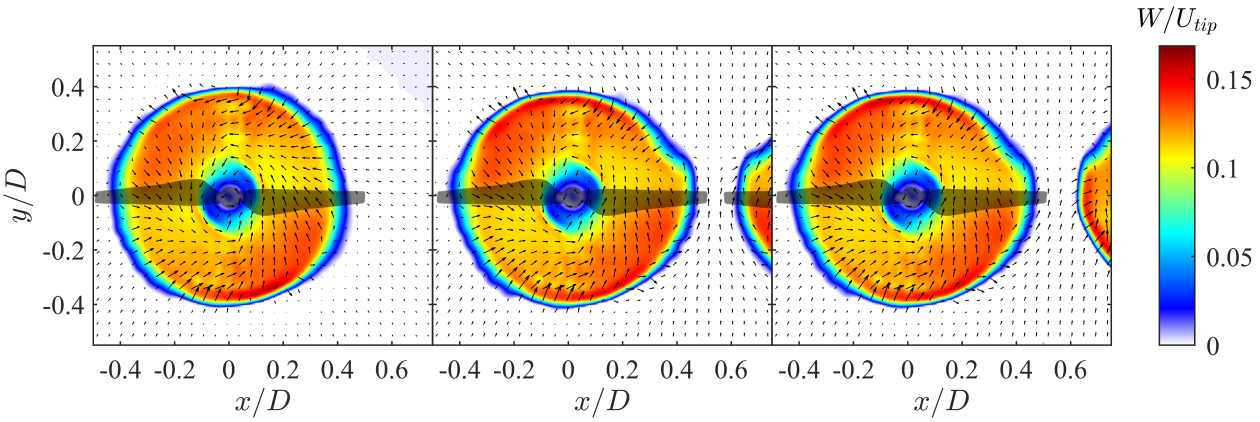

Fig. 6 Velocity plots

The momentum flux of the single propeller case and the two dual propeller cases taken at 4860 RPM is outlined in Fig. 7a. The momentum flux of all propeller cases was found by performing the aforementioned momentum thrust analysis on one propeller across various phase-locked angles. The differences in momentum flux between the two phase-locked cases is minimal. The momentum flux of the dual propeller cases appears to be a cyclic function of phase angle, fluctuating by up to 5% of the single propeller case. Phase-offset appears to have a minimal impact on the momentum flux of interacting propellers; there is little difference in average momentum flux and deviation in fluctuations are less than 1% between the two cases.

Unexpectedly, the dual propeller case momentum flux is higher than for the single propeller case, with a maximum increase of 4.9% and average increase of 2.2%. This is contrary to results found by other researchers, who reported drops in thrust with decreased propeller spacings by 3-4% [7, 8, 17, 25]. The increase in the flux of momentum through the measurement plane mirrors the region of larger axial flow between the propeller tips for the dual propeller cases, as was outlines in Fig. 6. Correcting the momentum balance by accounting for pressure acting on the control surface could answer why the momentum flux was larger for the dual propeller cases. It can be seen, however, that phase offset has little effect on the thrust fluctuations of interacting propellers.

The thrust and momentum flux of a single propeller plotted against RPM is compared to the measurements made by Zawodny et al. [24] in Fig. 7b. There is good agreement between the measured thrust and the results from Zawodny, with measurements within 5%. The momentum flux from the SPIV measurements is lower than both the thrust measurements and the data published by Zawodny by as much as 8%, as was also seen in Fig. 7a. Correcting the momentum balance by accounting for pressure acting on the control surface could account for this deficit.

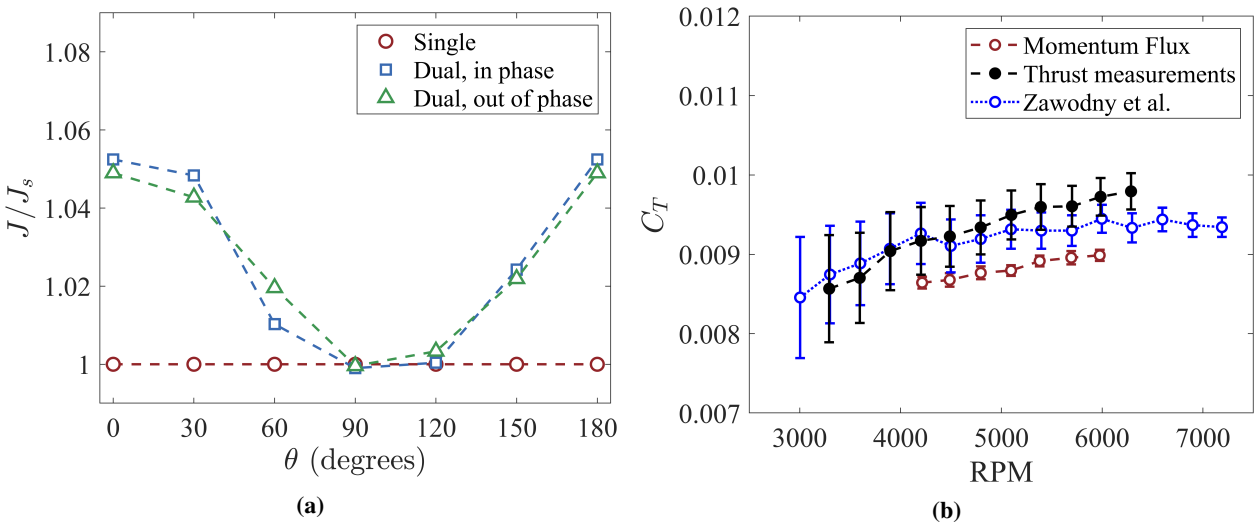

Fig. 7 Phase-locked fluctuations of momentum flux as a function of phase angle (a) and thrust measurements compared to the integrals of momentum flux and to results by Zawodny et al. [24] (b).

IV. Conclusion

Experiments exploring the effect of phase offset on interaction propellers were performed using PIV and SPIV systems. Tip vortex locations and peak vorticities were tracked and plotted for the various phase offset cases. The trajectories of the dual cases were altered when compared to the single. The tip vortices of the dual cases decayed 55% more rapidly than the single. There was little distinguishable differences between the tip vortices between the phase offset cases, however. The integral of momentum flux was found for across a full propeller revolution and compared across the phase offset tests. Fluctuations of up to 5% of the single propeller momentum flux were found for the dual propeller cases, but there was little difference between the phase offset cases. This method was validated by performing traditional thrust measurements using a thrust stand and compared to other published data. While the thrust measurements had good agreement with other published data, the momentum flux was consistently around 6-8% lower than the thrust measurements. This deficit is hypothesized to be due to not accounting for pressure acting on the control surface. It is concluded that the potential benefits of controlling propeller phase offset can be realized with negligible effects on propeller flow features and thrust fluctuations.

References

[1] Moore, M. D., "Misconceptions of Electric Aircraft and their Emerging Aviation Markets," *52nd Aerospace Sciences Meeting*, American Institute of Aeronautics and Astronautics, Reston, Virginia, 2014, pp. 1–17. https://doi.org/10.2514/6.2014-0535, URL https://arc.aiaa.org/doi/10.2514/6.2014-0535.

[2] Mcswain, R. G., Glaab, L. J., and Theodore, C. R., "Greased Lightning (GL-10) Performance Flight Research – Flight Data Report," Tech. Rep. November 2017, NASA, Hampton, 2017. URL https://ntrs.nasa.gov/archive/nasa/casi.ntrs.nasa.gov/

20180000765.pdf.

[3] Ko, Y.-Y. A., Mason, W. H., Grossman, B., Schetz, J. A., Haftka, R. T., and Kapania, R. K., "The Multidisciplinary Design Optimization of a Distributed Propulsion Blended-Wing-Body Aircraft," Ph.D. thesis, Virginia Tech, apr 2003.

[4] Gohardani, A. S., "A synergistic glance at the prospects of distributed propulsion technology and the electric aircraft concept for future unmanned air vehicles and commercial/military aviation," *Progress in Aerospace Sciences*, Vol. 57, 2013, pp. 25–70. https://doi.org/10.1016/j.paerosci.2012.08.001, URL http://dx.doi.org/10.1016/j.paerosci.2012.08.001https://linkinghub.elsevier.com/retrieve/pii/S0376042112000735.

[5] Stoll, A. M., Bevirt, J., Moore, M. D., Fredericks, W. J., and Borer, N. K., "Drag Reduction Through Distributed Electric Propulsion," *14th AIAA Aviation Technology, Integration, and Operations Conference*, American Institute of Aeronautics and Astronautics, Reston, Virginia, 2014, pp. 16–20. https://doi.org/10.2514/6.2014-2851, URL https://arc.aiaa.org/doi/10.2514/6.2014-2851.

[6] Yoon, S., Lee, H. C., and Pulliam, T. H., "Computational Analysis of Multi-Rotor Flows," *54th AIAA Aerospace Sciences Meeting*, American Institute of Aeronautics and Astronautics, Reston, Virginia, 2016, pp. 1–11. https://doi.org/10.2514/6.2016-0812, URL https://ntrs.nasa.gov/search.jsp?R=20160004754https://arc.aiaa.org/doi/10.2514/6.2016-0812.

[7] Shukla, D., Hiremath, N., and Komerath, N. M., "Low Reynolds Number Aerodynamics Study on Coaxial and Quad-Rotor," *2018 Applied Aerodynamics Conference*, American Institute of Aeronautics and Astronautics, Reston, Virginia, 2018, pp. 1–13. https://doi.org/10.2514/6.2018-4118, URL https://arc.aiaa.org/doi/10.2514/6.2018-4118.

[8] Shukla, D., and Komerath, N., "Low Reynolds number multirotor aerodynamic wake interactions," *Experiments in Fluids*, Vol. 60, No. 4, 2019, p. 77. https://doi.org/10.1007/s00348-019-2724-3, URL http://link.springer.com/10.1007/s00348-019-2724-3.

[9] Alvarez, E. J., and Ning, A., "High-Fidelity Modeling of Multirotor Aerodynamic Interactions for Aircraft Design," *AIAA Journal*, Vol. 58, No. 10, 2020, pp. 4385–4400. https://doi.org/10.2514/1.J059178, URL https://doi.org/10.2514/1.J059178https://arc.aiaa.org/doi/10.2514/1.J059178.

[10] Lee, H., and Lee, D.-j. J., "Rotor interactional effects on aerodynamic and noise characteristics of a small multirotor unmanned aerial vehicle," *Physics of Fluids*, Vol. 32, No. 4, 2020, p. 047107. https://doi.org/10.1063/5.0003992, URL http://aip.scitation.org/doi/10.1063/5.0003992.

[11] Schenk, "Computational Investigation of the Effects of Rotor-on-Rotor Interactions on Thrust and Noise," Ph.D. thesis, Brigham Young University, 2020.

[12] Afari, S., and Mankbadi, R. R., "Simulations of Noise Generated by Rotor-Rotor Interactions at Static Conditions," *AIAA Scitech 2021 Forum*, American Institute of Aeronautics and Astronautics, Reston, Virginia, 2021, pp. 1–15. https://doi.org/10.2514/6.2021-1986, URL https://arc.aiaa.org/doi/10.2514/6.2021-1986.

[13] de Vries, R., van Arnhem, N., Sinnige, T., Vos, R., and Veldhuis, L. L., "Aerodynamic interaction between propellers of a distributed-propulsion system in forward flight," *Aerospace Science and Technology*, Vol. 118, 2021, p. 107009. https://doi.org/10.1016/j.ast.2021.107009, URL https://linkinghub.elsevier.com/retrieve/pii/S1270963821005198.

[14] Stokkermans, T. C. A., Usai, D., Sinnige, T., and Veldhuis, L. L. M., "Aerodynamic Interaction Effects Between Propellers in Typical eVTOL Vehicle Configurations," *Journal of Aircraft*, Vol. 58, No. 4, 2021, pp. 815–833. https://doi.org/10.2514/1.C035814, URL https://arc.aiaa.org/doi/10.2514/1.C035814.

[15] Zhou, W., Ning, Z., Li, H., and Hu, H., "An Experimental Investigation on Rotor-to-Rotor Interactions of Small UAV Propellers," *35th AIAA Applied Aerodynamics Conference*, American Institute of Aeronautics and Astronautics, Reston, Virginia, 2017, pp. 1–16. https://doi.org/10.2514/6.2017-3744, URL https://arc.aiaa.org/doi/10.2514/6.2017-3744.

[16] Ning, Z., "Experimental investigations on the aerodynamic and aeroacoustic characteristics of small UAS propellers," Ph.D. thesis, Iowa State University, Digital Repository, Ames, jan 2018. https://doi.org/10.31274/etd-180810-6057, URL https://lib.dr.iastate.edu/etd/16427/.

[17] Shukla, D., and Komerath, N., "Multirotor Drone Aerodynamic Interaction Investigation," *Drones*, Vol. 2, No. 4, 2018, p. 43. https://doi.org/10.3390/drones2040043, URL http://www.mdpi.com/2504-446X/2/4/43.

[18] Westerweel, J., Elsinga, G. E., and Adrian, R. J., "Particle Image Velocimetry for Complex and Turbulent Flows," *Annual Review of Fluid Mechanics*, Vol. 45, No. 1, 2013, pp. 409–436. https://doi.org/10.1146/annurev-fluid-120710-101204, URL https://www.annualreviews.org/doi/10.1146/annurev-fluid-120710-101204.

[19] Tinney, C. E., and Sirohi, J., "Multirotor Drone Noise at Static Thrust," *AIAA Journal*, Vol. 56, No. 7, 2018, pp. 2816–2826. https://doi.org/10.2514/1.J056827, URL https://arc.aiaa.org/doi/10.2514/1.J056827.

[20] Patterson, A., Gahlawat, A., and Hovakimyan, N., "Propeller Phase Synchronization for Small Distributed Electric Vehicles," *AIAA Scitech 2019 Forum*, American Institute of Aeronautics and Astronautics, Reston, Virginia, 2019, pp. 1–14. https://doi.org/10.2514/6.2019-1458, URL https://arc.aiaa.org/doi/10.2514/6.2019-1458.

[21] Pascioni, K., and Rizzi, S. A., "Tonal Noise Prediction of a Distributed Propulsion Unmanned Aerial Vehicle," *2018 AIAA/CEAS Aeroacoustics Conference*, American Institute of Aeronautics and Astronautics, Reston, Virginia, 2018, pp. 1–18. https://doi.org/10.2514/6.2018-2951, URL http://arc.aiaa.orghttps://arc.aiaa.org/doi/10.2514/6.2018-2951.

[22] Pascioni, K. A., Rizzi, S. A., and Schiller, N., "Noise Reduction Potential of Phase Control for Distributed Propulsion Vehicles," *AIAA Scitech 2019 Forum*, American Institute of Aeronautics and Astronautics, Reston, Virginia, 2019, pp. 1–16. https://doi.org/10.2514/6.2019-1069, URL http://arc.aiaa.orghttps://arc.aiaa.org/doi/10.2514/6.2019-1069.

[23] Wieneke, B., "PIV uncertainty quantification from correlation statistics," *Measurement Science and Technology*, Vol. 26, No. 7, 2015. https://doi.org/10.1088/0957-0233/26/7/074002.

[24] Zawodny, N. S., Boyd, D. D. J., and Burley, C., "Acoustic Characterization and Prediction of Representative, Small-Scale Rotary-Wind Unmanned Aircraft System Components," *American Helicopter Society (AHS) Annual Forum*, 2016. URL https://ntrs.nasa.gov/citations/20160009054.

[25] Veismann, M., and Gharib, M., "High Fidelity Aerodynamic Force Estimation for Multirotor Crafts in Free Flight," *AIAA Scitech 2020 Forum*, American Institute of Aeronautics and Astronautics, Reston, Virginia, 2020, pp. 1–17. https://doi.org/10.2514/6.2020-0303, URL https://arc.aiaa.org/doi/10.2514/6.2020-0303.